Climate Data Record (CDR) Program

Climate Algorithm Theoretical Basis Document (C-ATBD)

RSS Version 3.3 MSU/AMSU-A
Mean Layer Atmospheric Temperature

REVISION HISTORY

Rev.	Author	DSR No.	Description	Date
1	Carl Mears, Remote Sensing Systems	DSR-225	Initial Submission to CDR Program	1/18/2013

TABLE of CONTENTS

LIST of FIGURES

LIST of TABLES

Search Word online help for "Add or delete captions" for assistance with this table

1.   Introduction

1.1   Purpose

The purpose of this document is to describe the algorithm submitted to the National Climatic Data Center (NCDC) by Remote Sensing Systems that will be used to create the RSS Version 3.3 MSU/AMSU-A Mean Layer Atmospheric Temperature Climate Data Record (CDR), using the MSU and AMSU instruments on NOAA, NASA, and EUMETSAT polar orbiting satellites. The actual algorithm is defined by the computer program (code) that accompanies this document, and thus the intent here is to provide a guide to understanding that algorithm, from both a scientific perspective and in order to assist a software engineer or end-user performing an evaluation of the code.

1.2   Definitions

Following is a summary of the symbols used to define the algorithm.

T_b = Brightness Temperature.   (1)

T_{Tar} = Temperature of Hot Calibration Target   (2)

A = Brightness Temperature Offset   (3)

α = Target Factor   (4)

β = scene Temperature factor   (5)

fov = field of view index (1-11 for MSU, 1-30 for AMSU   (6)

1.3   Document Maintenance

We anticipate that periodic updates to the algorithm and dataset will occur. This could be (for example) when data from additional satellites are included in the dataset, or when improvements to the algorithm are developed. Any update (beyond simply extending the dataset each month) will be given a new version number, and a new version of the ATDB will be generated.

2.   Observing Systems Overview

2.1   Products Generated

This CDR contains four data products. Each product is an intercalibrated radiance of microwave emission by thick layers of the atmosphere. For convenience, the radiance is expressed in temperature units, because in corresponds the weighted average of atmospheric temperature. The vertical weights are given by the weighting function for each product, shown in Fig. 2 below. The four products are listed below.

Table 1: Products contained in this CDR

Product	Approximate Vertical Extent
TLS (Temperature Lower Stratosphere)	12 – 26 km
TTS (Temperature Troposphere Stratosphere	3 – 20 km
TMT (Temperature Middle Troposphere)	Surface – 15 km
TLT (Temperature Lower Troposphere)	Surface – 8 km

2.2   Instrument Characteristics

2.2.1   Basic Description

Both MSU and AMSU are cross-track scanning radiometers that measure the upwelling radiance (brightness temperature) at different view angles as they scan the earth perpendicular to the satellite subtrack. They are both "step and integrate" instruments that move a scanning mirror to a new position and then make an averaged radiance measurement over a fixed integration time. After making a measurement at each earth viewing position, a two-point calibration is performed by rotating the mirror to view cold space and then a calibration target whose unregulated temperature is monitored with multiple precision thermistors. MSU views the earth at 11 view angles separated by 9.47 degrees, yielding a range of view angles from 0.0 for the nadir view, to 47.35 degrees for the two views furthest from nadir (Kidwell, 1998). Each scan, including the two calibration measurements, takes 25.6 seconds. On the earth's surface, this corresponds to earth incidence angles ranging from 0.0 degrees to approximately 56.19 degrees. MSU has a half-power beam width of 7.5 degrees, corresponding to a nadir spot size on the earth of 110 x 110 km, expanding to 178 x 322 km for the near-limb view due both to the increased distance from the spacecraft and to the oblique Earth incidence angle. The AMSU instruments have significantly higher spatial resolution, viewing the earth at 30 viewing angles separated by 3.33 degrees, with view angles ranging from 1.67 degrees to 48.33 degrees (Goodrum et al., 2000). Each scan takes 8 seconds. The view angles correspond to Earth incidence angles ranging from 1.88 degrees to 57.22 degrees. The half-power beam width of the AMSU instrument is 3.3 degrees, yielding a nadir spot size of 48 x 48 km, expanding to 80 x 150 km for the near-limb views. For channels TMT, TTS and TLS, we use

an average the central 5 MSU views, giving a swath width of approximately 640 km. For AMSU5 (TMT) and AMSU7 (TTS), we choose to use the central 12 fields of view (views 10-21), yielding a swath width of approximately 660 km, close to the MSU swath width for the central 5 views, thus keeping the spatial sampling similar to that for MSU. For AMSU9 (TLS), differences in the measurement frequency between MSU and AMSU made it necessary to use a set of 8 views (views 7-10 and 21-24) with larger incidence angles, resulting in a wider measurement swath with a stripe missing from its center.

2.2.2   Temperature Weighting Functions

By choosing measurement frequencies where the atmosphere is (almost) opaque, the upwelling radiation measured by microwave sounders is representative of the temperature of thick layers of Earth's atmosphere. We use a temperature weighting function to describe the relative contribution of each atmospheric layer to the observed brightness temperature T_b,

$$T_b = W_S T(0) + \int_0^{TOA} W(z) T(z) dz, \qquad (1)$$

where W_s is the surface weight, $T(z)$ is the temperature at height z, and $W(z)$ is the temperature weighting function, and the integral extends from the surface to the top of the atmosphere (TOA). The surface weight and the temperature weighting functions are dependent on the atmospheric absorption coefficient $\kappa(z)$ as a function of height z, the surface emissivity e_s, and the Earth incidence angle θ (Ulaby et al., 1981). The surface weight is given by the product of e_s and the attenuation from the surface to the top of the atmosphere,

$$W_s = e_s e^{-\tau(0,\infty)\sec\theta}, \qquad (2)$$

where

$$\tau(z_1, z_2) = \int_{z_1}^{z_2} \kappa(z) dz \qquad (3)$$

is the zenith optical depth for a layer that extends in height from z_1 to z_2, with $z_2 = \infty$ representing the top of the atmosphere. The weighting function is given by

$$W(z) = \kappa(z) T(z) \sec\theta e^{-\tau(z,\infty)\sec\theta} + \kappa(z) T(z) \sec\theta e^{-\tau(0,z)\sec\theta} (1-e_s) e^{-\tau(0,\infty)\sec\theta}. \qquad (4)$$

The first term is due to radiation emitted in the upward direction attenuated by the absorption of the intervening atmosphere. The second term is due to radiation emitted in the downward direction propagating to the surface and then being reflected upward, with attenuation along both the downward and upward paths. Increasing the zenith angle, and thus the path length through the atmosphere, increases both the emission by each

layer and the absorption terms. When combined, these effects cause the surface weight to be reduced and the peak of the temperature weighting function to move higher in the atmosphere.

Both MSU and AMSU make observations within a complex of oxygen emission lines near 60 GHz, whose width varies rapidly as a function of pressure, primarily due to collision-induced broadening. In the stratosphere, each line is clearly separated from it neighbors. As the pressure increases, the lines begin to broaden and merge together. By 300 hPa, the lines have merged into a single broad line with the MSU and AMSU measurement frequencies on the lower shoulder (see Fig. 1). Because the line width in the stratosphere is significantly less than the measurement bandwidths, it is necessary to perform radiative transfer calculations at a number of frequencies within each measurement band, and average these results together to obtain an accurate weighting function for each MSU/AMSU channel. This is particularly true for MSU channels 3 and 4, and for the corresponding AMSU channels 7 and 9. Below, we discuss each pair of the 3 sets of corresponding MSU and AMSU channels separately.
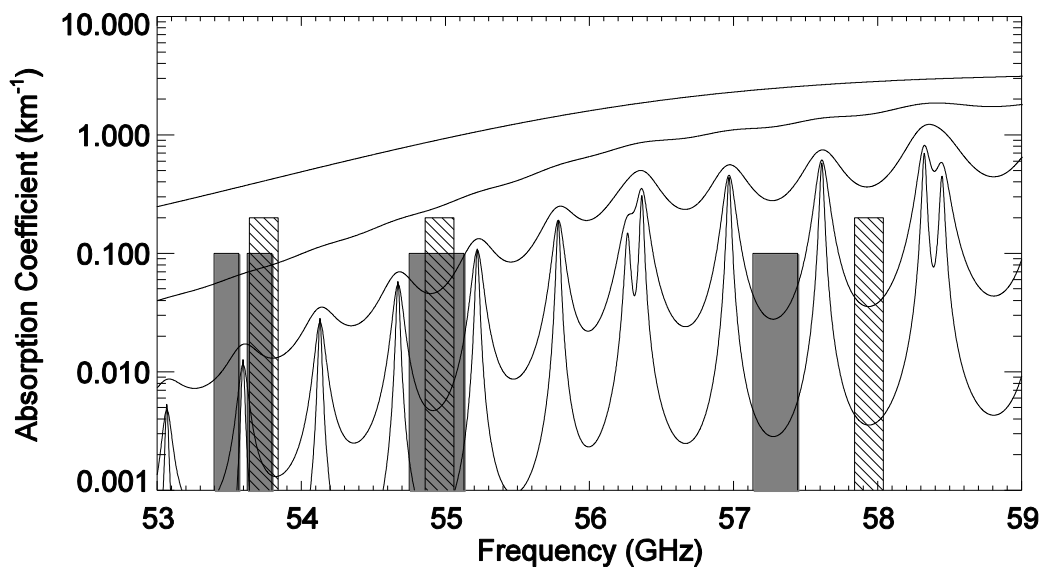
Figure 1:   The lines show the absorption coefficient as a function of frequency for 5 representative pressures (1000 (highest line), 300, 100, 30, and 10 hPa (lowest line). At high pressure, the individual absorption lines merge into a single broad line due to pressure broadening, while at low pressure the individual lines are still distinct, making the bandwidth of each measurement band important. The rectangles show the MSU (filled with diagonal lines) and AMSU (grey) measurement bands for the channels described in the text. (The height of the rectangles has no meaning, and serves to help separate the bands visually).

2.2.2.1   MSU2 and AMSU5

AMSU Channel 5 (AMSU5) is a double sideband receiver sensitive to two sidebands at 53.71 and 53.48 GHz, each with a bandwidth of 170 MHz. MSU channel 2 (MSU2) is a single sideband receiver with sensitivity at 53.74 GHz with a bandwidth of 200 MHz (see Fig. 1). In Figure 2a and 2b, we plot vertical weighting functions for the mean of the central 5 views of MSU2, and the mean of the central 12 views of AMSU5 for simulated land and ocean views using the 1976 U.S. Standard Atmosphere. These calculations were made using a radiative transfer model based on Rosenkranz (1998;1993) and our model of
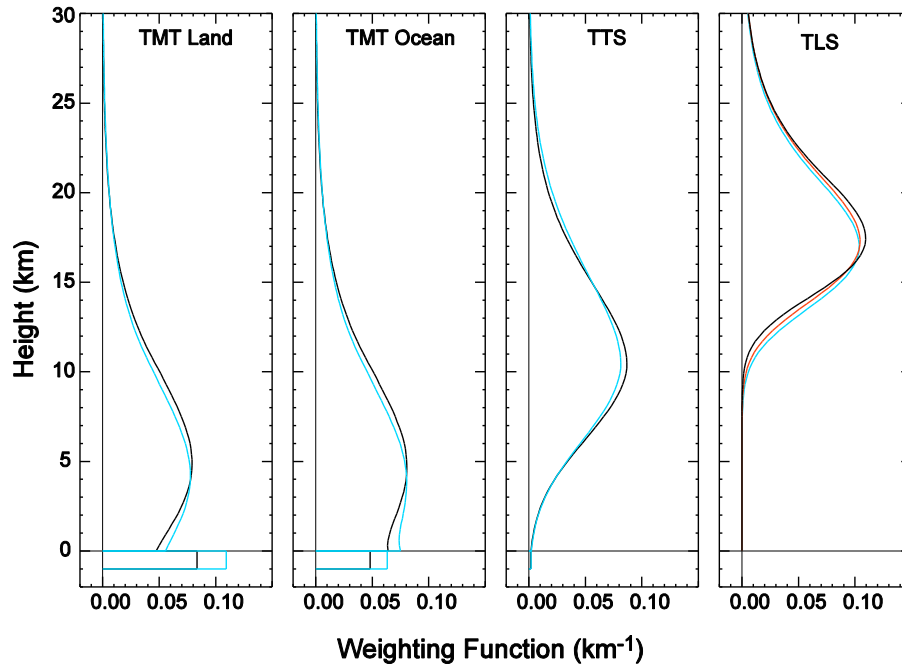
Figure 2: Vertical weighting functions for each MSU and AMSU channel. The MSU weighting functions (which use the central 5 views) are shown in black, and the corresponding AMSU weighting functions (using the central 12 views) are shown in blue. The boxes below zero height represent the surface weight. For TMT, land and ocean weighting functions are shown separately – for the other two channels the land and ocean weighting functions are almost identical to each other. Note the lower peak and increased surface weight for AMSU TMT (channel 5) relative to MSU (channel 2). This leads to an increase in brightness temperature that must be removed empirically before merging data from the two different instruments. There is also a large difference between the weighting functions for AMSU TLS (channel 9) and MSU (channel 4). We use an off-nadir set of AMSU views, whose weighting function is shown in red, to help reduce the differences before merging.

the ocean surface (Wentz and Meissner, 2000). Land surface emissivity was assumed to be 0.9, independent of incidence angle, an approximation which is supported by measurements at 37 GHz and 85 GHz (Prigent et al., 2000). The resulting weighting functions for AMSU5 peak about 500 meters closer to the surface, and the contribution of the surface is increased by about 35% relative to the MSU2 weighting function. Taken together, these changes result in a brightness temperature increase for AMSU5 relative to MSU2 of between 1.0 K and 3.0 K, depending on the surface type and local atmospheric profile. These differences must be removed before the AMSU results can be merged with the previous MSU data -- see section 4e for a description of our method.

2.2.2.2   MSU3 and AMSU7

AMSU7 is sensitive to a single band centered to 54.94 GHz, with a bandwidth of 380.5 MHz, and MSU3 is sensitive to a single band centered at 54.96 GHz, with a bandwidth of 200 MHz. Because the center frequencies are so similar, the shape of the weighting function in the low to mid troposphere is very similar between the two channels. The greater width of the AMSU7 measurement band leads to significantly more weight in the lower stratosphere than for MSU3 when the central 5 (MSU) and central 12 (AMSU) views are used (see Fig 2c), since more of the wings of the individual lines are sampled at low pressure by the wider measurement band (see Fig 1). This difference leads to a brightness temperature decrease for AMSU 7 relative to MSU 3 of several tenths of a degree K. The difference is greatest in the tropics where the vertical lapse rate is the largest in the upper troposphere and lower stratosphere. These differences are also removed using a method similar to that used for MSU2/AMSU5.

2.2.2.3   MSU4 and AMSU9

AMSU9 is sensitive to a single band centered at 57.29 GHz, with a bandwidth of 310 MHz, while MSU4 is sensitive to a single band at 57.94 GHz, with a bandwidth of 200 MHz. It can be seen in Fig. 1 that the AMSU9 measurement band is located between a lower-frequency pair of absorption lines than MSU4 and thus shows a lower absorption coefficient at all pressures. This leads to a weighting function for AMSU9 that peaks about 500m lower in the atmosphere than the weighting function for MSU4. Because the mean lapse rate is relatively small in the region where the difference between the weighting functions is largest, the average temperature difference is only a few tenths of a degree K. However, the difference in weighting functions leads to large differences in both the seasonal cycle and the response to stratospheric warming events in the polar regions. Unlike the case for the lower frequency channels, these differences are not well accounted for by a simple location and time-of-year dependent difference, due both to the non-periodic nature of the stratospheric warmings, and to the greater difference between the weighting functions. Instead, before removing the residual differences empirically, we choose to better match the intra-annual behavior of the two channels by using a set of AMSU views with larger incidence angles, and thus longer slant paths through the atmosphere that moves the peak of the weighting function further above the surface.

2.2.2.4   MSU2 and AMSU5: TLT

Direct MSU2 and AMSU5 measurements have the disadvantage that a significant amount of the weighting function is in the stratosphere. Because the stratosphere is cooling, this tends to cancel the warming signal from the troposphere. Spencer and Christy (1992) devised a weighted difference constructed from near-limb MSU2 that extrapolates the weighting function closer to the surface. The MSU TLT dataset is based on a weighted difference of MSU views,

$$T_{TLT-MSU} = T_{B,3} + T_{B,4} + T_{B,8} + T_{B,9} - 0.75\left(T_{B,1} + T_{B,2} + T_{B,10} + T_{B,11}\right). \qquad (5)$$

This combination of views nearly cancels the stratospheric influence and moves the peak of the temperature weighting function lower in the troposphere (Spencer and Christy, 1992). In Fig. 3, we show the 2LT temperature weighting functions for land and ocean surfaces on the same vertical scale as Fig. 2.
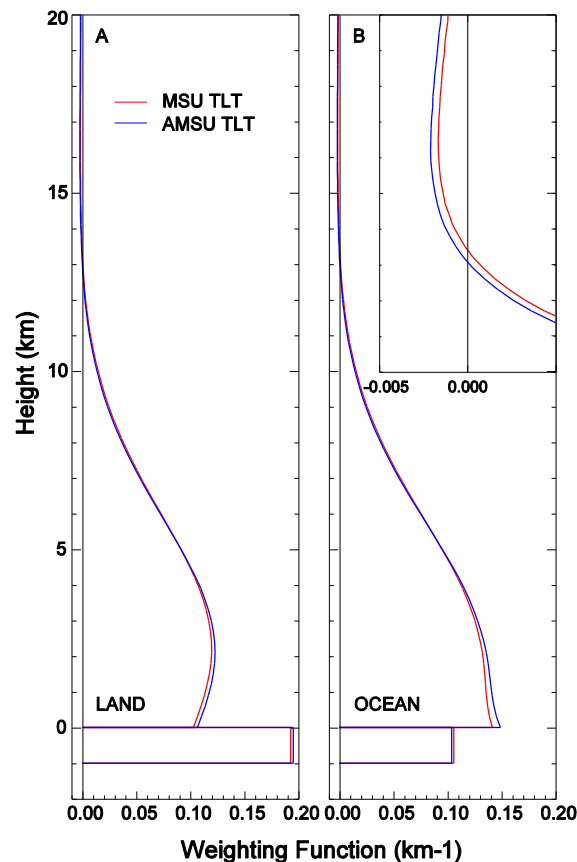
Figure 3: TLT temperature weighting functions as a function of altitude for MSU and AMSU. As in Fig. 2 the rectangle at the bottom of each panel represents the weight due to surface emission. (A) Weighting functions over land. (B) Weighting functions over ocean. In the inset, we show the two weighting functions on an expanded scale for high altitude.

Our task now is to find a combination of AMSU measurements that provide the same brightness temperatures as would be found using the combination of MSU measurements presented in Eq. 3. We use a regression method to obtain weights a_{fov} for the AMSU views. The set of equations to be solved are given by

$$\sum_{fov} c_{fov} T_{MSU}\left(fov\right) = \sum_{fov} a_{fov} T_{AMSU}\left(fov\right) \qquad (6)$$

$T_{AMSU}(fov)$ are the AMSU brightness temperatures for each field of view *fov*, and $T_{MSU}(fov)$ are the MSU brightness temperatures. The MSU weights c_{fov} are those given in Eq. 3. Additional equations of the form k(a_{fov} -a_{fov+1}) = 0 were added to the set of equations before their solution was determined. The effect of these equations is reduce the effects of noise by introducing a non-parametric smoothness constraint on the a's as a function of fov.   We solved this equation simultaneously using monthly zonal averages from NOAA-14 (MSU) and NOAA-15 (AMSU) as input data. The zonal averages were calculated over 5 degree zonal bands, and were calculated separately for land and ocean scenes and for each *fov*. Land areas with surface height averaged over the 2.5 degree by 2.5 degree cell that exceed a threshold altitude of 1500 meters were excluded from the averages to reduce contamination from surface emission. The land and ocean averages were used to form separate equations to deduce a set of a_{fov}'s that produce a good brightness temperature match for both land and ocean scenes independently. Each equation was weighted according to the area of the earth that it represented, i.e. for a given zonal band, the land equation was weighted by the land area in that band, and the ocean equation was weighted by the ocean area in that band.   The a_{fov}'s were constrained to be equal to the corresponding weight on the opposite side of the swath, and the weights for the central 14 views were set to zero so that the derived AMSU product would cover roughly the same part of the swath as the MSU product. (We also performed the calculation with only the central 12 views excluded; this would result on an improved match to the MSU measurement swath. The resulting weight for the innermost included view was so small that we decided to exclude it.) In Table 2 we show the regressed values for the weights a_{fov}, and in Fig. 4 we plot the MSU and AMSU weights as a function of incidence angle.   The resulting temperature weighting functions are plotted in Fig. 3 for both

Table 2 AMSU TLT FOV weights

FOV	Weight
a_{15}, a_{16}	0.00
a_{14}, a_{17}	0.00
a_{13}, a_{18}	0.00
a_{12}, a_{29}	0.00
a_{11}, a_{20}	0.00
a_{10}, a_{21}	0.00
a_9, a_{22}	0.00
a_8, a_{23}	-0.25
a_7, a_{24}	0.40
a_6, a_{25}	1.17
a_5, a_{26}	1.61
a_4, a_{27}	1.41
a_3, a_{28}	0.44
a_2, a_{29}	-1.14
a_1, a_{30}	-2.64
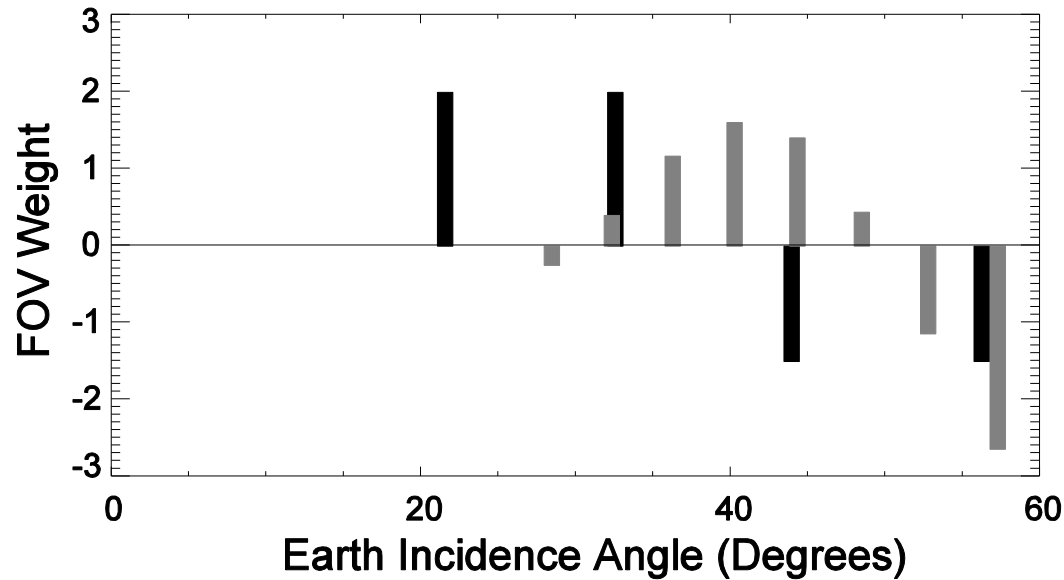
Figure 4 Field of view (fov) weights used to calculate TLT plotted as a function of incidence angle for both MSU (dark bars) and AMSU (light bars).

ocean and land surfaces, along with the original MSU derived weighting functions.

The validity of this procedure was evaluated in two ways. First, we studied the residual error between the weighted, zonally and monthly averaged MSU and AMSU combinations. The standard deviation of the difference between these two combinations is about 0.12K, about three times the error we expect due to differences in temporal sampling between the two instruments. Thus these difference suggest that though it is impossible to exactly match these weighting functions with a single set of AMSU weights, a reasonably good match can be obtained. Second, Fig. 3 indicates that there is also a good match between the two weighting functions derived using these weights and the U. S. standard atmosphere, showing that our combination of views physically matches the temperature weighting of the original MSU 2LT product. While the differences in weighting functions between the two instruments makes a globally-valid, exact solution based solely on view weighting impossible, the weighting procedure developed here minimizes the magnitude of the location-dependent differences between MSU and AMSU measurements. These location-dependent differences will be removed empirically in a later step.

In Table 3, we summarize the MSU and AMSU channels that are combined to form our new datasets, and the names given the resulting channels, following Christy et al. (2000). These names will be used in the remainder of the document. It is important to note that although the MSU2/AMSU5 combination is called TMT or Temperature Middle Troposphere, this channel also has significant (5% to 15%) weight in the stratosphere, so that any tropospheric warming may be partly masked by the contribution of stratospheric cooling.

Table 3: MSU and AMSU Channel for each final product

MSU Channel	AMSU Channel	Combined Channel	Acronym
2	5	Temperature Lower Troposphere	TLT
2	5	Temperature Middle Troposphere	TMT
3	7	Temperature Troposphere Stratosphere	TTS
	9	Temperature Lower Stratosphere	TLS

3.   Algorithm Description

3.1   Algorithm Overview

The CDR algorithm begins with raw radiance data from each satellite, performs a number of quality checks and pre-merge adjustments. The most important of these is an adjustment for changes in local measurement time. The algorithm then computes monthly-averaged maps for each satellite from the adjusted data. These average maps are then used to derive fine calibration adjustments for each satellite.   The adjustments are applied, and then the data from the different satellites are merged together using simple averaging.

3.2   Processing Outline

The following outlines the routine processing currently done to perform the monthly updates. For earlier MSU satellites, geolocation errors in the L1B files made it necessary to perform a number of additional steps.

3.2.1   Data Download

For NOAA and EUMETSAT satellites, L1B data files are downloaded from NOAA's CLASS system. For AQUA, data is downloaded from Goddard Earth Sciences Data and Information Services Center. Both downloads are accomplished using a data pull.

3.2.2   MSU Processing

3.2.2.1   MSU L1B to RSS L2C Processing

This part of the processing is covered by the flow chart shown in Fig. 5.

The starting point for this part of the data is NOAA L1B data files from the CLASS system. First, the data in the individual NOAA L1B files is checked for nonsense data and duplicatated data, and then the data is assembled into RSS L1B files. Each RSS L1B files contains data from 1 orbit. This part of the processing is performed by a fortran program called ***MSU_L1B_ingest.exe***. The output of this program are single orbit files such as NOAA-06_r00037.L0.gz. (the "L0" part of the name refers to Level 0, and is left over from a previous level naming scheme).

These files are then processed by a C++ program called ***Generate_MSU_L1A_Swath_Data_V02_1.exe***. This program calculates brightness temperatures from raw counts, and applies adjustments for orbital height and the local measurement time, and also calculates an adjustment to refer each measurement to nadir. For the early satellites, orbital information is also check, and erroneous data is fixed using a two-line element interpolation scheme. The output of this program is RSS L2A files, such as NOAA-06_r00037.L1A.gz. (The L1A in the program name and file name is left over from a previous data level naming scheme.)

The L2A files are then assembled into gridded monthly files by a fortran program called ***update_MSU_L2C.exe***. The output of this program are files called MSU_*nn*_Chan_*m*_Monthly_Hist_144_72_N5_V3_0.dat, where *nn* is the satellite number, and *m* is the channel
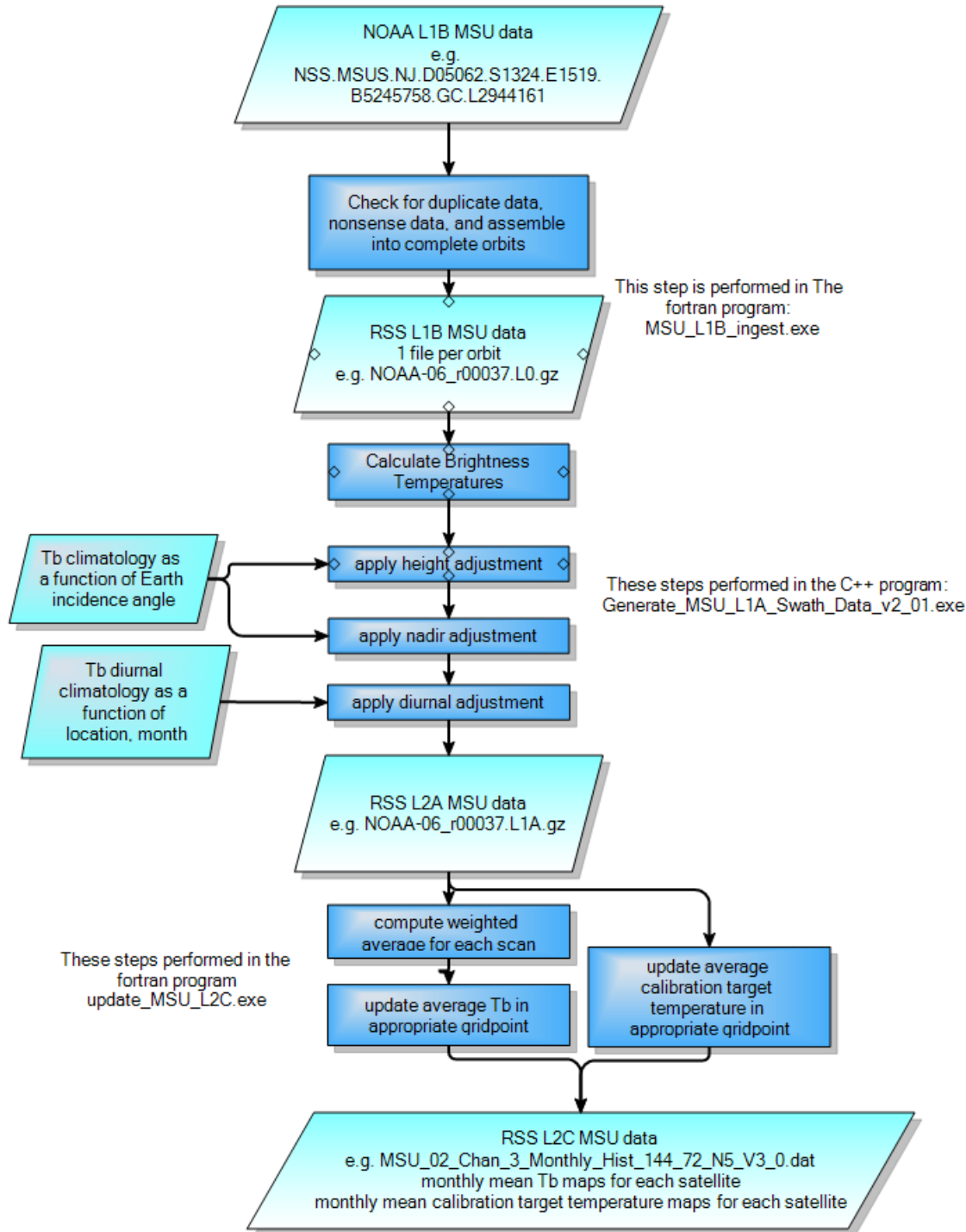
Figure 5. Flow Chart for MSU L1B to L2C processing.

3.2.2.2   MSU RSS L2C Cross-Calibration and Merging

This part of processing is covered by the flow chart shown in Fig. 6.

All processing is performed by the IDL routine ***grpt_merge_msu_only_v3_3.pro***. The routine names in the flowchart are called by this top-level program.

The starting point are the MSU L2C files of monthly gridded temperature data created in the last step (3.2.2.1). The files are read into the computer for all 9 MSU satellites (4 Satellites for MSU channel 3) in the subroutines

   read_all_monthly_maps_msu_only_v3_3.pro and (for the TLT case)

   read_all_monthly_maps_msu_only_tlt_v3_3.pro.

The next step is to calculate global means from the monthly maps, and use these means in a regression procedure to calculate values for the target factors. This is performed in ***calc_tf_from_grpt_maps.pro***.

These target factors the then applied to the data in ***apply_tf_to_grpt_maps.pro***, resulting in an intermediate adjusted dataset in the variable tb_arr_adj.

Then latitude dependent offsets are calculated in ***calc_offsets_from_grpt_maps.pro***, and the results smoothed in the north-south direction in ***smooth_offsets.pro***. The smoothed offsets are then applied to tb_arr_adj in ***apply_offsets_to_grpt_maps.pro***.

Then, a single scene temperature factor is calculated and applied to each satellite in ***calc_single_TbF_from_grpt_map.pro***

The data from the different satellites are then merged together using simple averaging, using code in the main routine.

The final results are written to a msu level 3 file using the routine ***write_msu_only_merged_Tbs_144_72_netcdf_3_3.pro.*** These files are named RSS_Tb_Maps_ch_*m*_v3_3_*nnn*.dat, where m is the msu channel, and nnn is a sub-version number. The sub-version for the final dataset is 011.
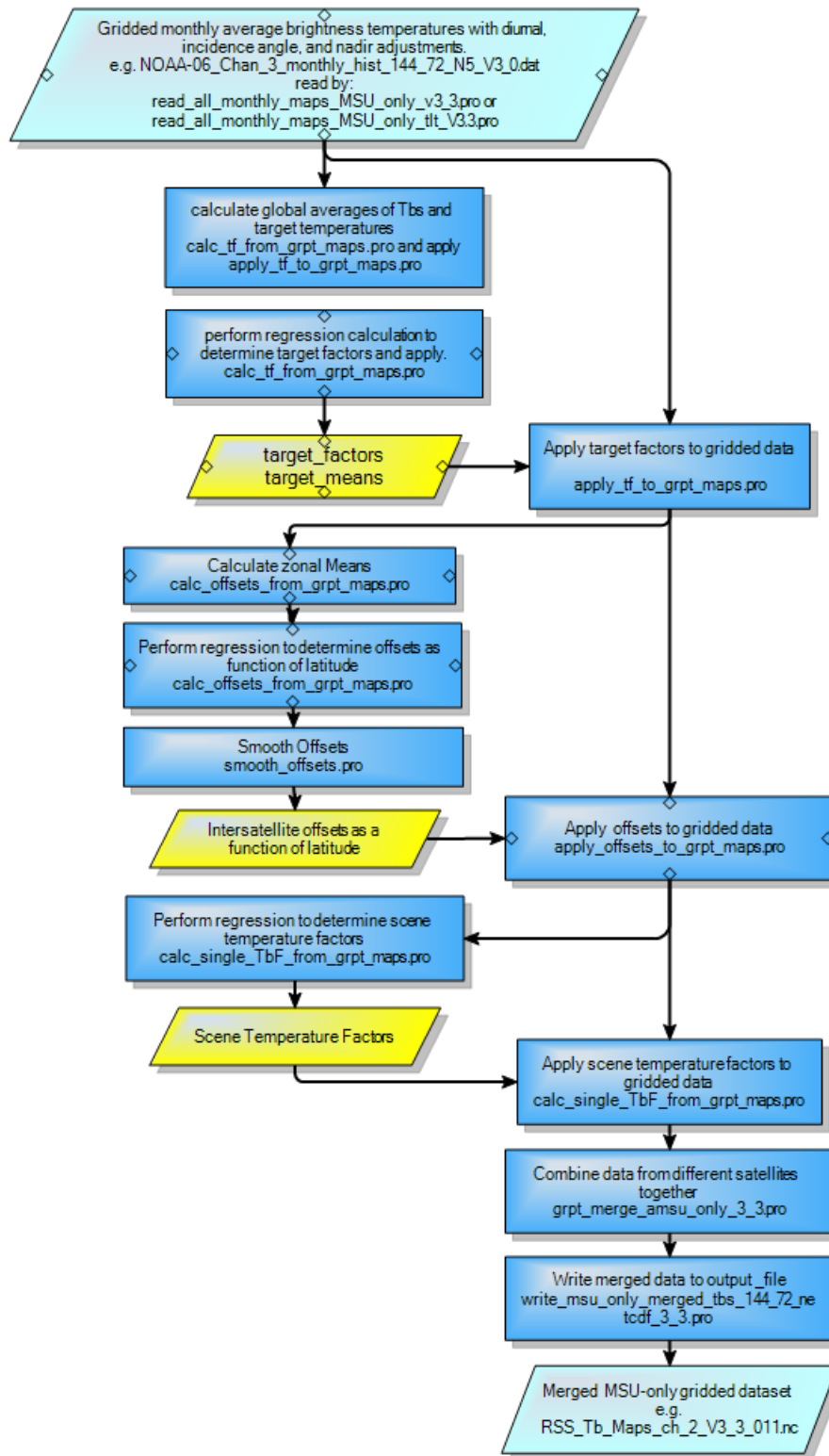
Figure 6 Flow chart for MSU intersatellite calibration and merging.

3.2.3   AMSU Processing

3.2.3.1   AMSU L1B to RSS L2C Processing

This part of the processing is covered by the flow chart shown in Fig. 7.

The starting point for this part of the data is NOAA L1B data files from the CLASS system. First, the data in the individual NOAA L1B files is checked for nonsense data and duplicated data, and then the data is assembled into RSS L1B files. Each RSS L1B files contains data from 1 orbit.

For NOAA and EUMETSAT data, this part of the processing is performed by a FORTRAN program called ***AMSU_orbitify.exe***. The output of this program are single orbit files such as NOAA-15_r00037.L0.gz. (the "L0" part of the name refers to Level 0, and is left over from a previous level naming scheme).

For NASA AQUA data, this part of the processing is performed by a IDL program called ***orbitify_AQUA_V5_driver.pro***. (The V5 refers to the NASA version number).

For the NOAA and EUMETSAT data, these files are then processed by a C++ program called ***AMSU_L1B_to_L2A.exe***. This program calculates brightness temperatures from raw counts, and applies adjustments for orbital height and the local measurement time, and also calculates an adjustment to refer each measurement to nadir. The output of this program are RSS L2A files, such as NOAA-15_r60000.L2A.gz. (There is one L2A file for each channel. Channels are denoted by location in the directory structure, not the file name.)

NASA AQUA data is already in radiance, so all that needs to be done is to add the diurnal and angle adjustment information. This is done using the fortran program ***AMSU_AQUA_L2A_add_corrections.exe***

The L2A files are then assembled into gridded monthly files by a fortran program called ***update AMSU_L2C_choose_diurnal.exe***. The output of this program are files called NOAA-nn_Chan_cc_yyyy_mm_N12_V3_02.CCM3.dat, where *nn* is the satellite number, *cc* is the channel, yyyy is the year, and mm is the month. CCM3 refers to the use of the CCM3 model output for the diurnal adjustment.
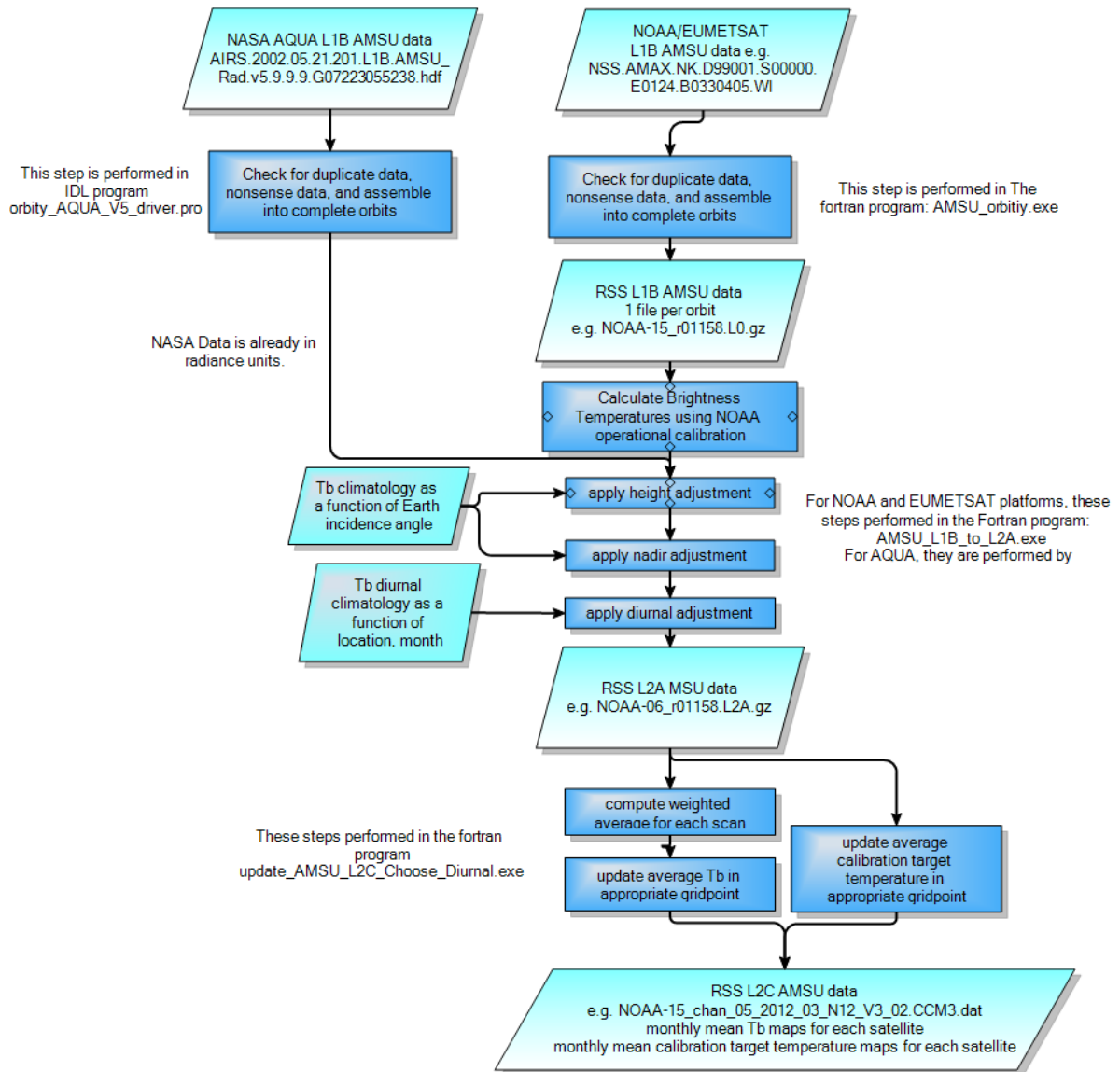
Figure 7. Flow Chart for AMSU L1B to L2C processing.

3.2.3.2   AMSU RSS L2C Cross-Calibration and Merging

This part of the processing is covered by the flow chart shown in Fig. 8.

All processing is performed by *grpt_merge_amsu_only_v3_3.pro*. The routine names in the flowchart are called by this top-level program.

The starting point are the AMSU L2C files of monthly gridded temperature data created in the last step (3.2.2.1). The files are read into the computer for all 6 MSU satellites in the subroutine *read_all_monthly_maps_amsu_only_v3_3.pro*

Each monthly map is then checked to make sure that it has enough observations to be valid in the subroutine *check_grpt_maps_amsu_v3_3.pro*

The next step is to calculate global means from the monthly maps, and use these means in a regression procedure to calculate values for the target factors. This is performed in *calc_tf_from_grpt_maps_AMSU.pro*.

These target factors the then applied to the data in *apply_tf_to_grpt_maps_AMSU.pro*, resulting in an intermediate adjusted dataset in the variable tb_arr_adj.

Then latitude dependent offsets are calculated in *calc_offsets_from_grpt_maps_AMSU.pro*, and the results smoothed in the north-south direction in smooth_offsets.pro. The smoothed offsets are then applied to tb_arr_adj in *apply_offsets_to_grpt_maps_AMSU.pro*.

The data from the different satellites are then merged together using simple averaging, using code in the main routine (*grpt_merge_amsu_only_3_3.pro*).

The final results are written to an AMSU level 3 file using the routine *write_amsu_only_merged_Tbs_144_72_netcdf_3_3.pro.* These files are named RSS_Tb_Maps_ch*mm*_v3_3_*nnn*.dat, where mm is the AMSU channel, and nnn is a sub-version number. The sub-version for the AMSU data used in the final dataset is 011.
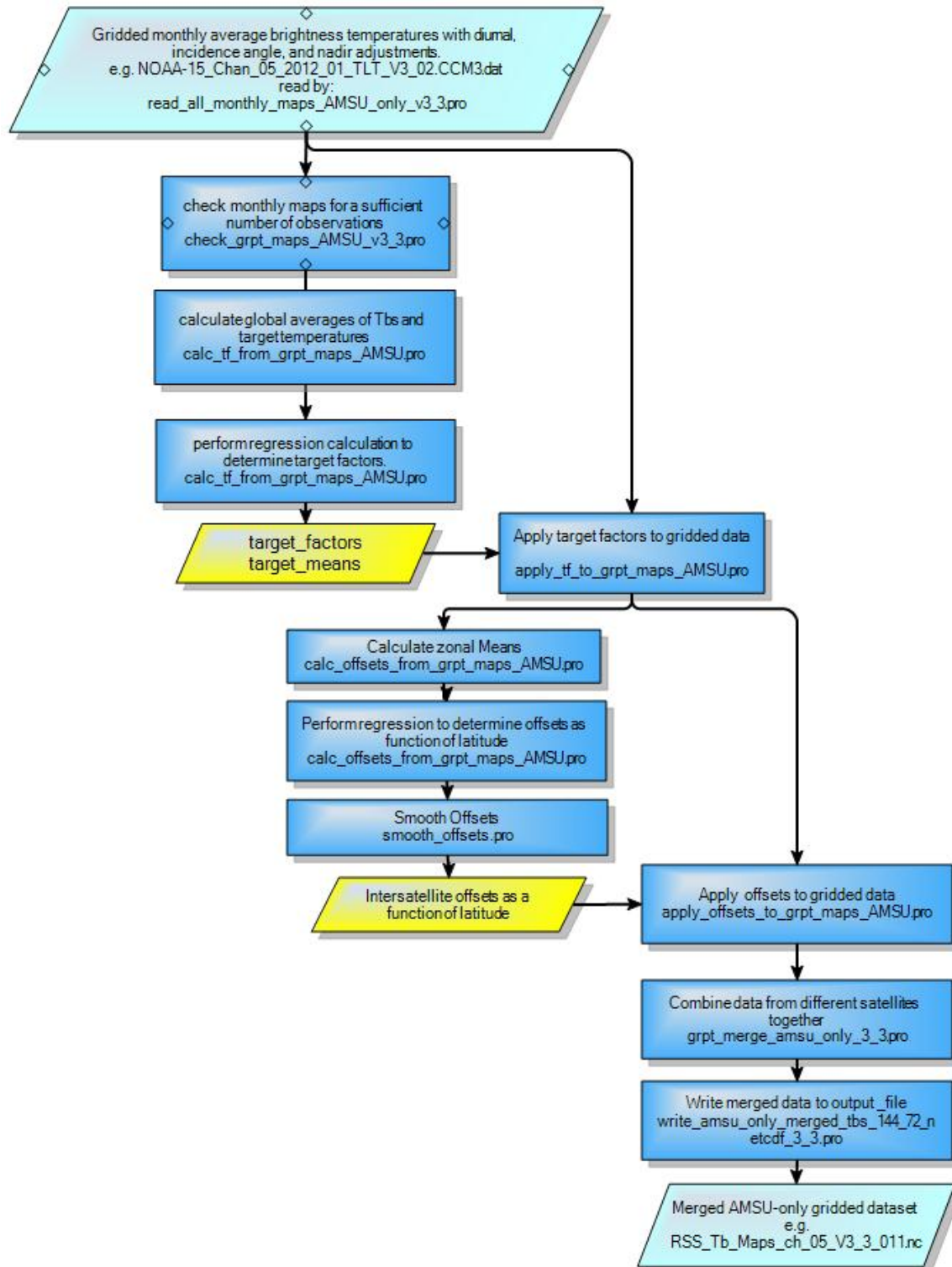
Figure 8. Flow chart for AMSU intersatellite calibration and merging.

3.2.4   Combining MSU and AMSU

This part of the processing is covered by the flow chart shown in Fig. 9. All processing is done in the IDL code **combine_msu_amsu_merged_maps_3_3.pro**. The starting point for this part of the processing is the MSU and AMSU level 3 merged monthly maps created in sections 3.3.2.2 and 3.3.3.2. These are read in, and then month and location dependent offsets are calculated using a 2-harmonic fit to the differences series. For TLS, these offsets are then smoothed by fitting each monthly map using a spherical harmonic basis $Y_{l,m}$, with l ranging from 0 to 9. These offsets are then applied to the AMSU data so that it corresponds to the MSU data. The MSU and AMSU data are then combined using simple averaging. The resulting merged product is then adjusted so that it refers to local midnight using the routines **chng_to_midnight.pro** and **chng_to_midnight_TLT.pro**. The final results are then written in netcdf by the routine **write_msu_amsu_merged_Tbs_144_72_netcdf_3_3.pro.**
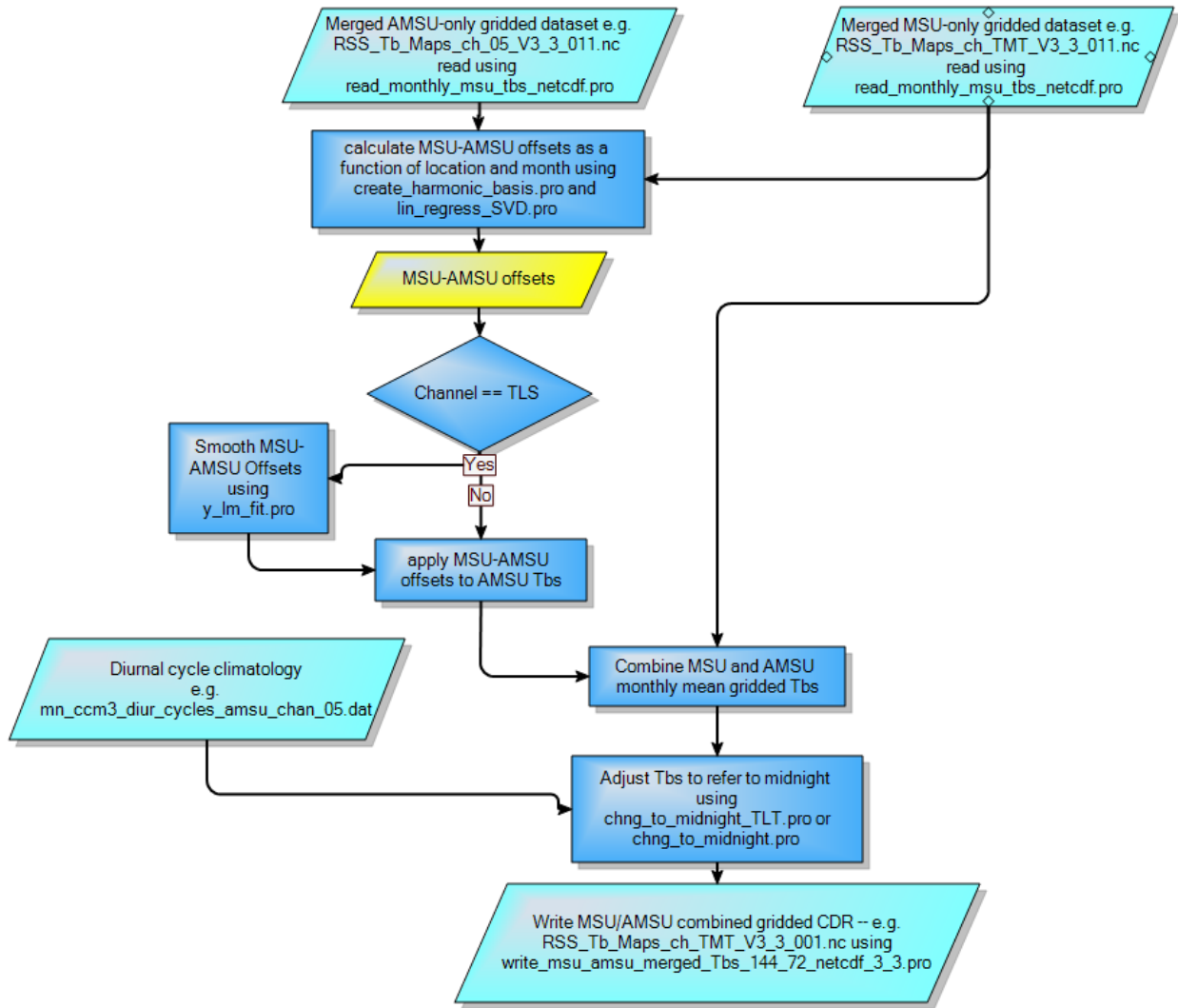
Figure 9. Flow chart for combining MSU and AMSU measurements.

3.3   Algorithm Input

3.3.1   Primary Sensor Data

Most of the raw sensor data is MSU and AMSU L1B data files which are freely accessible from NOAA's Comprehensive Large Array-Data Stewardship System (CLASS, system http://www.class.ncdc.noaa.gov). For AMSU, each file contains data from roughly 1 orbit, is approximately 2 MB in size, and is in a binary format that must be decoded by the user's computer program.

The exceptions to this are AMSU data from the AQUA satellite. For AQUA, we use L2A data, which is available from the Goddard Earth Sciences Data and Information Services Center (http://disc.sci.gsfc.nasa.gov). We use the AMSU data in Version 5 of the AIRS dataset. These files are arranged in data granules (240 per day), which we cut apart and re-arrange into single orbit files.

We have investigated use of the data from the 9 MSU instruments, and the AMSU instruments on NOAA-15, 16, and 18, AQUA and MetOp-A. The premature malfunction of the AMSU instrument on the NOAA-17 platform yields a data set too short in duration to contribute significantly to a long-term time series. Since 3 instruments (MSU on NOAA-14, and the three AMSUs) continued to operate after its failure, its use would bring little new long-term information to the data product. After evaluation, we also decided to exclude NOAA-16 data from our combined dataset. The details leading to this decision are discussed in Mears et al., 2009a. Our final dataset used data from all 9 MSU instruments, NOAA-15, NOAA-18, AQUA and MetOP-A.

3.3.2   Ancillary Data

The algorithm requires several ancillary data files. These are listed below.

Diurnal Climatology—e.g. mn_ccm3_diur_cycles_amsu_chan_05.dat

purpose:	calculating adjustments for changes in local measurement time. One file is available for each AMSU channel.
format:	binary
version:	N/A
size:	175 MB
location:	Remote Sensing Systems
access:	on request
references:	

Earth Incidence Angle Climatology—e.g. amsu_tbs_from_ncep_LTM_month_02.dat

purpose:	calculating adjustments for changes in Earth Incidence Angle and calculating adjustments so that the brightness

temperature corresponds to nadir.   One file is available for each AMSU channel.

format: binary
version: N/A
size: 3.7 MB
location: Remote Sensing Systems
access: on request
references:

AMSU Equator Crossing Times – e.g. NOAA_K.eqx

purpose: Contains equator crossing time and longitude for each orbit. These are used for calculating measurement time adjustments. These are assembled from the NOAA navigation files available at http://www.osdpd.noaa.gov/data/ppp/NAVIGATION/. The AQUA version is assembled from information in the AQUA L2A files.
format: text
version: N/A
size: 1 – 3 MB
location: Remote Sensing Systems
access: on request
references:

MSU Orbital Elements – e.g. Ancillary_Data\TLE\noaa-06.txt

purpose: Correct errors in MSU navigation that are present in the L1B files from CLASS. "Two-line" orbital elements were obtained from celestrak (http://celestrak.com). In some cases, it was necessary to interpolate the elements to account for missing data.
format: text
version: N/A
size: 1 – 3 MB
location: Remote Sensing Systems
access: on request
references:

3.3.3   Derived Data

Not Applicable

3.3.4   Forward Models

Describe any forward models used as input to the algorithm. Indicate "Not applicable" if there are no forward models.

No forward models are directly used by the algorithm. We use a microwave radiative transfer and surface emissivity model to produce look up tables of brightness temperature climatology from general circulation model output.

3.4   Theoretical Description

3.4.1   Physical and Mathematical Description

3.4.1.1   Earth Incidence Angle Adjustments

For the near-nadir view subsets (MSU2_N5 and AMSU5_N12), each observation is adjusted to correspond to the nadir view (limb adjustment) so that the difference between measurements at different incidence angles is diminished, thereby reducing sampling noise in the final product[1]. This adjustment also removes the small effects of changes in incidence angle both due to variations in Earth's radius of curvature and due to variations in orbital height, and thus the effects of orbital decay. The adjustment is made using simulated brightness temperatures calculated from an NCEP-reanalysis-based atmospheric profile climatology (Kalnay et al., 1996;Mears et al., 2003). We found that the global average of the difference between the modeled and measured temperatures was not zero or symmetric about nadir. For MSU, we found that we had to include an additional term that was well-modeled as an instrument roll (Mears et al., 2003). For the AMSU instruments, we found that after performing the model-based nadir adjustment, an additional empirical correction $T_0(fov)$ for each field of view (not well described by an instrument roll) was needed to force the adjusted globally averaged brightness temperatures to be independent of field of view.

$$T_{Adj}(nadir) = T_{AMSU}(fov) + T_{Mod}(nadir) - T_{Mod}(fov) + T_0(fov) \qquad (5)$$

T_{Adj} is the adjusted temperature, T_{AMSU} is the measured temperature, and T_{mod} is the simulated brightness temperature from the NCEP-based climatology, interpolated in location at time of year to match the observation undergoing adjustment. The empirical corrections $T_0(fov)$ are typically a few tenths of a Kelvin, and are independent of location on the earth and time of year, and thus has a negligible effect on long-term behavior. These are largest near the two ends of the scan, and are likely to be due to spill-over effects.

3.4.1.2   Local Measurement Time (Diurnal) Adjustments

Using 5 years of hourly output from the CCM3 climate model (Kiehl et al., 1996), we created a diurnal climatology for the MSU channels 2-4 and AMSU channels 5,7 and 9 as a function of earth location, time of day, time of year, and incidence angle using the

---

[1] For AMSU9, which uses a combination of 8 limb views, the adjustment to nadir is not performed, since it would result in lowering the effective weighting function of the view combination. For this channel, we use a

methods described in (Mears et al., 2002). This diurnal climatology was then used to adjust each measurement so that it corresponds to local noon.

$$T_{Adj}(noon) = T_{AMSU}(fov) + T_{Mod}(noon) - T_{Mod}(t) \qquad\qquad (6)$$

The adjustments are largest for MSU2 and AMSU5, because of the contribution of surface emission to these channels. Surface emission can have a large diurnal signal, particularly in arid land regions. These regions dominate the global average of the MSU2 and AMSU5 adjustments. In Fig. 6, we show time series of the global (-82.5 to 82.5) mean of the adjustments applied to each MSU and AMSU channel for the NOAA-14 (MSU) and NOAA-15 (AMSU) satellites. Because the characteristics of the diurnal cycle vary with time of year and location, there are significant annual and semiannual signals in the adjustment for each channel. The diurnal adjustment for AMSU5 is about 40% larger than that for MSU2 for the same crossing time. This is because 1) the surface contribution for AMSU5 is about 35% larger than MSU2, and 2) the AMSU5 weighting function has more weight near the bottom of the troposphere, where the diurnal cycle is large over land areas. It is possible that significant errors are present in the CCM3-derived diurnal cycles, since errors have been demonstrated to be present in the diurnal cycle of cloud cover and precipitation, and the diurnal cycle in near-surface air temperature appears to be too small in the model (Dai and Trenberth, 2004).

3.4.1.3   Constructing Monthly Gridded Maps

Gridded (2.5 x 2.5) monthly average maps are constructed using all valid data for a given month/satellite. The choice of instrument views and view weights for each product is discussed in section 2.2.2 above. In each case, the chosen views are combined using the appropriate weights, and this weighted average contributes to the mean in any grid cell that contains the center of any of the fields of view. For TMT, TTS, and TLS, data from the ascending and descending nodes are computed separately. For TLT, the left and right side of the swath is computed separately. The reasons for the different approach for TLT are explained in Mears and Wentz, 2009b. These gridded means are stored in separate files for each satellite/month/channel

3.4.1.4   MSU and AMSU Calibration Adjustments

Global averages of simultaneous measurements made by co-orbiting MSU instruments differ by both a time-invariant intersatellite offset and an additional term that is strongly correlated with the variations in temperature of the hot calibration target for each satellite. This effect was first noticed by Christy and coworkers (Christy et al., 2003). The exact physical cause of this small calibration error is not known. Possible causes include residual non-linearity in the radiometer response that was not adequately measured during ground calibration, or an error in the specification of the effective brightness temperature of the calibration target. The error in the specification of the effective calibration target temperature could be due to a combination of any or all of the following effects: (1) temperature gradients between the precision thermistors and the emitting surface, (2) errors in the calibrations of these thermistors, (3) a non-unit emissivity of the calibration target, or (4) antenna spillover around the target causing other

sources (either warm satellite parts or cold space) to be sensed during the calibration procedure. It is also possible that the source of error is due to changes in the temperature of the radiometer electronics that result in a change in receiver parameters. To first order, such changes are removed by the two-point calibration procedure, but changes in absolute noise levels, coupled with non-linearity in the receiver, could also result is the observed behavior. These various causes are difficult to separate using on-orbit analysis techniques, since they lead to similar behavior as a function of calibration target temperature (or instrument temperature, which closely tracks calibration target temperature) and scene temperature. The source of error may be a combination of several of these factors, including both non-linearity, temperature specification and instrument temperature effects. An additional complication is that any non-linearity in radiometer response may be dominated by cubic or other higher order terms, since the NOAA non-linearity correction procedure implemented in routine processing minimizes quadratic non-linearity by design.

All the types of errors discussed above also cause an error that depends on brightness temperature being sensed, or the scene temperature (Grody et al., 2004). Because the globally averaged seasonal cycle for each channel is relatively small, scene-temperature-related effects are small and difficult to separate from the much larger target temperature effects when global averages are considered. Our earlier work focused on global averages, and thus we omitted scene temperature effects. Scene temperature dependent errors may be an important contributor to latitude dependence of intersatellite offsets and are important in polar regions where the seasonal cycle in atmospheric temperature is very large.

Instead of attempting to determine the physical source of the calibration errors unambiguously, we use an empirical error model for brightness temperature incorporating the target temperature and scene temperature correlation,

$$T_{MEAS,i} = T_0 + A_i + \alpha_i T_{TARGET,i} + \beta_i T_{SCENE} + \varepsilon_i \tag{6}$$

where T_0 is the true brightness temperature, A_i is the temperature offset for the i-th instrument, α_i is a small multiplicative "target factor" describing the correlation of the measured antenna temperature with the temperature anomalies of the hot calibration target, $T_{TARGET,i}$. The parameter β_i describes the correlation of the calibration error with the scene temperature anomaly T_{SCENE}, and ε_i is an error term that contains additional uncorrelated, zero-mean errors due to instrumental noise and sampling effects. This model is an extension of the model used by both Christy et al. (2003), and Mears et al (2003) in that it now includes the scene temperature dependence. We find the scene temperature term necessary to reduce seasonally dependent intersatellite differences in the polar regions for the MSU series of satellites. The new model is also closely related to the physically-based error model proposed by Grody et al (2004). This relationship is described in the appendix of Mears et al 2009a.

A central question is whether the merging parameters (the A_i's, α_i's, and β_i's) should be constant for each satellite, or be allowed to vary with earth location (e.g. latitude). After extensive analysis (See Mears et al, 2009a) we reached the conclusion that

the target temperature factors and scene temperature factors should be location invariant, while the offsets are allowed to vary with latitude.

The values of the calibration parameters (offsets, target factors, and scene factors) are found using a series of regression calculations that explain differences between results from satellites making measurements at the same time using the error model.

Each gridded monthly map is checks to make sure it contains a sufficient number of observations. Satellite-Months that pass this test are used to construct a global-mean time series of brightness temperature and calibration target temperature for each satellite. Intersatellite differences and target temperatures are used to construct a system of equations

$$T_{MEAS,i} - T_{MEAS,j} = A_i - A_j + \alpha_i T_{TARGET,i} - \alpha_j T_{TARGET,j},$$

Where $T_{MEAS,i}$ is the measured brightness temperature for the ith satellite, A_i is the offset for the ith satellite, α_i is the target factor for the ith satellite, and $T_{TARGET,i}$ is the calibration target temperature for the ith satellite. One equation is constructed for each month with a pair of observind satellites. This system is solved using singular value decomposition to obtain values for the target factors.

The next step is to calculate the latitude dependent satellite offsets. For each zonal band, we solve a system of equations given by

$$T_{MEAS,i,k} - T_{MEAS,j,k} = A_{i,k} - A_{j,k} + \alpha_i T_{TARGET,i,k} - \alpha_j T_{TARGET,j,k} \quad ,$$

which is a version of Eq. 7 generalized so that each equation describes the difference between measurements made by the ith and jth satellites for the *kth zonal band*, where the $A_{i,k}$'s are allowed to vary with latitude. The target factors α_i are fixed to the values found in the previous step, and the equations are solved for each zonal band. To prevent a singular set of equations, we must set the overall offset to a fixed value. We choose to set the offset for NOAA-10 to zero for all latitudes. This assumption affects the absolute values of the measurements made, but has no effect on the long-term in brightness temperature. The offset values for each satellite are then smoothed in the north-south direction using a mean-of-seven "boxcar" smooth.

When we apply the target factors and offset determined in the previous steps to the data and evaluate the intersatellite differences, we find that (for MSU) there are significant seasonal-scale fluctuations near the poles, where the seasonal cycle is large, but not near the equator, where the seasonal scale is small. This suggests that part of the remaining differences is caused by a scene-temperature related calibration error. To remove this, we again take the difference between versions of Eq. 7 for each month that two or more satellites are observing simultaneously. Substituting the values already determined for the $A_{i,j}$'s and the α_i's, into

$$T_{ADJ,i,k} = T_{MEAS,i} - A_{i,k} - \alpha_i T_{TARGET,i,k},$$

and keeping the T_{SCENE} dependence from Eq. 6 we obtain a system of equations given by,

$$T_{ADJ,i,k} - T_{ADJ,j,k} = \beta_i T_{SCENE,i,k} - \beta_j T_{SCENE,j,k} = (\beta_i - \beta_j) T_{SCENE,k}$$

for each zonal band. We can replace $T_{SCENE,i,k}$ and $T_{SCENE,j,k}$ with $T_{SCENE,k}$ because the scene temperature is independent of the satellite index. T_{SCENE} is closely approximated by the measured antenna temperatures. To prevent noise in the measurements from unduly influencing the derived values for the β's, we use for T_{SCENE} an average scene temperature. This average is found by averaging the results from all satellites over the 1979-1998 period together to form an antenna temperature climatology that depends on latitude and month. These values are then used in the system of equations described by Eq. 8 to deduce the values for the β's. Since the β_i's only appear in the equations as differences between β's for different satellite their average value is arbitrary. We use singular value decomposition to choose the minimal-variance solution for the β_i's, since we want to change the data by the smallest possible amount. These adjustments are then applied to the MSU data. For AMSU, the scene temperature effect is too small to be concerned with, so the β_i's are set to zero for AMSU. The adjusted data for each type of satellite (MSU or AMSU) are then merged together using simple averaging for months when two or more satellites are operating at the same time.

3.4.1.5 MSU/AMSU merge

Because of the difference between the MSU and AMSU weighting functions for corresponding channels, there are small differences between the measured antenna temperatures that depend on the local atmospheric profile and surface temperature. We remove these differences on average by calculating the mean difference between MSU and AMSU measurements as a function of earth location and time of year. We then subtract the difference from the adjusted gridded monthly AMSU averages so that they match the corresponding MSU-only data. For MSU2/AMSU5, the spatial pattern in the difference is dominated by differences in surface type, i.e. land vs. ocean.   For MSU4/AMSU9, the spatial pattern in the differences showed the largest variability in the mid latitudes, where sampling error is important. We choose to reduce the effect of sampling error for channels MSU4/AMSU9 by smoothing the difference maps by fitting to spherical harmonics $Y_{L,M}$ using values of L up to 9, and M between –L and L. After the spatial/temporal adjustments are applied to the AMSU data, results from the two different instrument types are then merged, using simple averaging when data from both MSU and AMSU are present.

3.4.2   Numerical Strategy

Regression calculations are performed in double precision using singular value decomposition. This guards against numerical error in systems of equations that are close to being singular.

3.4.3   Calculations

See 3.4.1 above

3.4.4   Look-Up Table Description

3.4.4.1   Diurnal Climatology

For each channel, we have constructed a brightness temperature climatology as a function of location, time of day, time of year, and Earth incidence angle. The climatology was constructed by feeding 5 years of hourly climate model output (from CCM3) into a radiative transfer model to calculate an hourly gridded brightness temperature dataset. These data were averaged to construct the climatology. The climatology is used to adjust the measured brightness temperatures so that they correspond to measurements made at local noon, and to convert measurements at local noon to local midnight.

Here is a list and description of the files used:

MSU Versions:

The three files are:

MSU channel 2   mn_diur_cycles_chan_2_ccm3_128x64_local_time.dat

MSU channel 3   mn_diur_cycles_chan_3_ccm3_128x64_local_time.dat

MSU channel 4   mn_diur_cycles_chan_4_ccm3_128x64_local_time.dat

Each file contains a single binary array filled with 4-byte reals. The array dimensions are 6 X 12 x24 x 128 x 64. Byte order is little endian. Array ordering is FORTRAN standard, or column-major order.

The first index (6) corresponds to the Earth incidence angle.

The second index (12) refers to the month of the year.

The third index (24) refers to the hour of the day.

The fourth index (128) refers to the longitude grid box (2.8125 x 2.8125) degree grid.

The fifth index (64) refers to the latitude grid box (2.8125 x 2.8125) degree grid.

AMSU Versions:

The three files are:

AMSU channel 5   mn_ccm3_diur_cycles_amsu_chan_05.dat

AMSU channel 7   mn_ccm3_diur_cycles_amsu_chan_07.dat

AMSU channel 9   mn_ccm3_diur_cycles_amsu_chan_09.dat

Each file contains a single binary array filled with 4-byte reals. The array dimensions are 15 X 12 x24 x 144 x 72. Byte order is little endian. Array ordering is FORTRAN standard, or column-major order.

The first index (15) corresponds to the Earth incidence angle.

The second index (12) refers to the month of the year.

The third index (24) refers to the hour of the day, centered on the ½ hour.

The fourth index (144) refers to the longitude grid box (2.5 x 2.5) degree grid.

The fifth index (72) refers to the latitude grid box (2.5 by 2.5) degree grid.

3.4.4.2   Mean Brightness Temperature as a function of Earth incidence angle

For each channel, we have constructed a brightness temperature climatology for the nominal Earth incidence for each view angle for the instrument, in addition to the first and second derivatives with respect to changes in Earth incidence angle. The climatology is constructed as a function of position and time of year. This is used to calculate adjustments for changes in Earth incidence angle, and also to refer measurements to nadir. This table is constructed from NCEP long-term means using a radiative transfer model.

These are used to compute the angle corrections for the MSU and AMSU data. The Files contain the average brightness temperature for each location, nominal earth incidence angle, and month, along with the first and second derivatives with respect to incidence angle.

The files containing these tables are described below:

MSU Versions:

For MSU, there is a separate file for each month, channel, and surface type (land or ocean). Each file is named:

tbdata_CHz_Sx_yyyy_mm_topo_theta.dat

where z is the MSU channel (2, 3, or 4)

where the 'x' is the surface type

1 = Ocean

2 = Land

yyyy is the year (always 1996)

mm   is the month of the year (1-12)

Each file is a 73 x 144 x 3 x 6 x 2 flat binary array of 4 byte reals. Byte order is little endian. Array ordering is FORTRAN standard, or column-major order.

The spatial grid is "corner-centered", ranging from (-90.0,0.0)..(2.5,2.5)..(90.0,357.5)

The first dimension is the latitude

The second dimension is the longitude

The third dimension is the data type (1= Tb0, 2 = Tb1, 3 = Tb2, where

Tb = Tb0 + Tb1*(theta -theta_nom) + (Tb2/2.0)*(theta-theta_nom)^2

The fourth dimension is the angle index (0 = nadir, ... 5 = outermost)

The fifth dimension is the polarization (0 = v-pol, 1 = h-pol)

The nominal angles (theta_nom) for each angle index are as follows:

index	theta_nom
0	0.0
1	10.71
2	21.51
3	32.51
4	43.91
5	56.19

AMSU Versions:

These files contain simulated Tbs calculated from NCEP monthly averages for 1996. There is a separate directory for each AMSU channel.

The file names are

ncep_amsu_tbs_cc_yyyy_mm.dat

where cc denotes the channel, yyyy denotes the year, and mm the month each file contains a 3 x 15 x 144 x 73 x 2 flat binary array of 4 byte reals.

The first dimension is the data type (0 = Tb0, 1 = Tb1, 2 = Tb2, where

Tb = Tb0 + Tb1*(theta -theta_nom) + (Tb2/2.0)*(theta-theta_nom)^2.

The second dimension is the angle index, with the first angle being the near-

nadir view, and the last angle being the near-limb view.

The third dimension is the longitude.

The fourth dimension is the latitude.

(spatial grid is corner-centered, ranging from (-90.0,0.0)..(2.5,2.5)..(90.0,357.5))

The fifth dimension is surface type (0 = ocean, 1 = land).

The nominal angles (theta_nom) for each angle index are as follows:

index	view_nom	EIA_nom
0	1.666666	1.875947
1	5.000000	5.629541
2	8.333333	9.388301
3	11.666667	13.155880
4	15.000000	16.936250
5	18.333333	20.733890
6	21.666667	24.554020
7	25.000000	28.402830
8	28.333333	32.287970
9	31.666667	36.219100
10	35.000000	40.208800
11	38.333333	44.274040
12	41.666667	48.438570
13	45.000000	52.737200
14	48.333333	57.224260

Cross Track Corrections

For AMSU, additional, constant cross track corrections are applied.

For each satellite, channel, and cross-track scan position, a constant offset is applied. These are calculated by comparing the average values of the brightness temperature measured by the satellite with average simulated brightness temperatures calculated using data from NCEP long-term means.

The files are simple text files containing 30 values (one for each scan position, with the first value corresponding to the first scan position), and are named:

Sat_xx_Channel_yy_Cross_track_corrections.txt

Where "xx" is the satellite number (10-16) and yy is the channel number (05, 07, or 09).

3.4.5   Parameterization

None used.

3.4.6   Algorithm Output

The output of the algorithm is 4 netcdf files containing monthly averaged brightness temperatures in degrees Kelvin gridded in a 2.5 by 2.5 degree latitude/longitude grid. The entire dataset is reconstructed for each monthly update. An example filename is

uat4_tb_v03r03_avrg_chTMT_197812_201206.nc, where

v03r03 corresponds to the version number

TMT corresponds to the product (layer) name

197812 corresponds to the begin year and month, and

201206 corresponds to the end year and month.

Each file is in netcdf4 format, and is approximately 18 MB in size.

4. Test Datasets and Outputs

4.1 Test Input Datasets

There are no formal test datasets at this point.

4.2 Test Output Analysis

4.2.1 Reproducibility

Not Applicable

4.2.2 Precision and Accuracy

See 4.2.3

4.2.3 Error Budget

Organize the various error estimates into an error budget, presented as a table. Error budget limitations should be explained. Describe prospects for overcoming error budget limitations with future maturation of the algorithm, test data, and error analysis methodology.

We have performed an extensive error analysis using Monte-Carlo methods. Because of the significant correlations present in the estimated error, the error budget cannot be represented in table form with much meaning. We provide a large number (currently 100) error realizations via our website (www.remss.com). See Mears et al., 2011 for details.

5.   Practical Considerations

5.1   Numerical Computation Considerations

Nothing very fancy is done. As discussed above, regression calculations are done using SVD in double precision to reduce effects of numerical error.

5.2   Programming and Procedural Considerations

Most of the computer time is spent doing file input/output. Numerical speed is not an issue for routine daily and monthly updates. As the algorithm is configured at Remote Sensing Systems, roughly 1-2 hours per day is spent processing individual AMSU orbits for the previous day to RSS L2A format. Then, for each monthly update, 3-4 hours is spent assembling monthly maps (RSS L2C data) from the individual orbits. This is done for the 6 months before the current data to ensure that an orbits that are late to arrive at RSS are included. If this were not cone, the processing time would be significantly less.The merging step (L2C to L3) takes only a few minutes for each channel. A complete reprocessing of the entire dataset would likely take several weeks or a month for a single processor to perform, due to the large number of orbits involved. The is no theoretical reason that prevents simplistic parallelization of the algorithm (e.g. different orbits running on separate processors), though practical considerations, e.g. attempting to open a file that is already open and in use with access locked, may cause failures if this is attempted as the code is currently written.

5.3   Quality Assessment and Diagnostics

Historically, the largest source of anomalies has been failures in the download mechanism, which has led to insufficient data for one or more satellite months. This often manifests itself in the form of excessive noise in the final dataset, which can be seen by visual inspection of anomaly maps. These are now detected automatically in the merging code.

5.4   Exception Handling

See Section 5.3.

5.5   Algorithm Validation

Final results have been validated by comparing them to other MSU/AMSU datasets, measurements made by radiosondes, and by comparing changes in temperature to changes in total column water vapor.

5.6   Processing Environment and Resources

All processing takes place on a single laptop running windows XP pro 64 bit. Data is stored on a multi-terabyte, raided, enterprise class server running Windows Server 2008. Most processing takes place in IDL, except for some more data intensive tasks that

use Fortran. Downloading and file copying and overall process control is performed using python scripts.

6.   Assumptions and Limitations

There are a number of assumptions that were made during the development of our algorithm. Below we list the most important assumptions for each part of the algorithm.

6.1   Angle Corrections

Corrections for Earth Incidence Angle are made using long-term means generated from the NCEP reanalysis. We assume that these provide an accurate picture of the temperature structure of the atmosphere (i.e. mean temperature and lapse rate), and that the structure is constant in time. Violation of either of these assumptions could lead to errors as a function of Earth Incidence Angle.

6.2   Diurnal Corrections

Corrections for changes in local measurement time are made using a diurnal cycle climatology constructed using output from the CCM3 atmospheric model. We assume that the diurnal cycle is accurately depicted in this model, and that the Earth's diurnal cycle is stationary of the duration of our dataset. We have investigated the validity of these assumptions by comparing the CCM3 diurnal cycle to the diurnal cycle climatology from other models, and by assessing the difference between measurements made during the ascending and descending portions of the orbit (which are typically spaced by about 12 hours.) These suggest that possible errors in the diurnal cycle are non-zero and are likely to be the largest source of error for the tropospheric channels. See Mears et al., 2011 for more details.

6.3   Calibration Error Model

We assume that calibration errors are well described by our error model, presented in section 3.4.1.4, that is, that calibration errors are well characterized by constant offsets, and errors proportional to the calibration target and scene temperatures. In general, this seems to be the case, but there are calibration errors that our procedure could not detect. For example, if all satellites suffered from a calibration drift that changes linearly in time, our method (which is based on intersatellite differences) could not detect its presence.

We also assume that the calibration offsets depend only on latitude. We have uncovered evidence that suggests that separate offsets for land and ocean scenes could be advantageous.

We also provide a fixed calibration point by assuming that the calibration offsets for NOAA-10 are zero. The means that the absolute calibration is arbitrary, and that the absolute calibration error is probably on the order of 0.5K.

7.   Future Enhancements

7.1   Enhancement 1

Use of separate offsets for land and ocean scenes. This will reduce the tendency for the after the fit brightness temperature differences between satellites to depend on scene type.

7.2   Enhancement 2

Use of an ancillary data source (probably reanalysis output) to fix the absolute calibration (currently uncertain to +/- 0.5 K or so) using a clearly defined method.

8.   References

Christy, J. R., R. W. Spencer, W. B. Norris, W. D. Braswell and D. E. Parker, (2003) Error Estimates of Version 5.0 of MSU-AMSU Bulk Atmospheric Temperatures, *Journal of Atmospheric and Oceanic Technology, 20*(5), 613-629.

Dai, A. and K. E. Trenberth, (2004) The Diurnal Cycle and Its Depiction in the Community Climate System Model, *Journal of Climate, 17*, 930-951.

Goodrum, G., K. B. Kidwell and W. Winston, (2000), NOAA KLM user's guide, National Climatic Data Center.

Grody, N. C., K. Y. Vinnikov, M. D. Goldberg, J. T. Sullivan and J. D. Tarpley, (2004) Calibration of Multi-Satellite Observations for Climatic Studies: Microwave Sounding Unit (MSU), *Journal of Geophysical Research, 109*, doi:10.1029/2004JD005079.

Kalnay, E., M. Kanamitsu, R. Kistler, W. D. Collins, D. Deaven, L. Gandin, M. Iredell, S. Saha, G. White, J. Woollen, Y. Zhu, M. Chelliah, W. Ebisuzaki, W. Higgins, J. E. Janowiak, K. C. Mo, C. Ropelewski, J. Wang, A. Leetmaa, R. Reynolds, R. Jenne and D. Joseph, (1996) The NCEP/NCAR 40-Year Reanalysis Project, *Bulletin of the American Meteorological Society, 77*, 437-471.

Kidwell, K. B., (1998), NOAA Polar Orbiter Data Users Guide, National Climatic Data Center.

Kiehl, J. T., J.J.Hack, G.B.Bonan, B.A.Boville, B.P.Briegleb, D.L.Williamson, and P.J.Rasch (1996), Description of the NCAR Community Climate Model (CCM3), *report TN-420*, National Center for Atmospheric Research, Boulder, CO.

Mears, C. A., M. C. Schabel and F. J. Wentz, (2003) A Reanalysis of the MSU Channel 2 Tropospheric Temperature Record, *Journal of Climate, 16*(22), 3650-3664.

Mears, C. A., M. C. Schabel, F. J. Wentz, B. D. Santer and B. Govindasamy (2002), Correcting the MSU middle tropospheric temperature for diurnal drifts, paper presented at Proceedings of the International Geophysics and Remote Sensing Symposium,Toronto, Canada.

Prigent, C., J. P. Wigneron, W. B. Rossow and J. R. Pardo-Carrion, (2000) Frequency and Angular Variations of Land Surface Microwave Emissivities: Can We Estimate SSM/T and AMSU Emissivities From SSM/I Emissivities?, *IEEE Transactions on Geoscience and Remote Sensing, 38*(5), 2373-2386.

Rosenkranz, P., (1998) Water Vapor Microwave Continuum Absorption: A Comparison of Measurements and Models, *Radio Science, 33*(4), 919-928.

Rosenkranz, P. W., Absorption of microwaves by atmospheric gases, in Atmospheric Remote Sensing by Microwave Radiometry, edited by M. A. Janssen, pp. 37-90, John Wiley and Sons, New York, 1993.

Spencer, R. W. and J. R. Christy, (1992) Precision and Radiosonde Validation of Satellite Gridpoint Temperature Anomalies. Part II: A Tropospheric Retrieval and Trends During 1979-1990, *Journal of Climate, 5*, 858-866.

Ulaby, F. T., R. K. Moore and A. K. Fung, Microwave Remote Sensing: Active and Passive, Artech House, Norwood, MA, 1981.

Wentz, F. J. and T. Meissner, (2000), AMSR Ocean Algorithm, Version 2, vol. 121599A-1, p. 66, Remote Sensing Systems, Santa Rosa, CA.

Acronyms and Abbreviations

Acronym or Abbreviation	Meaning
AMSU	Advanced Microwave Sounding Unit
C-ATBD	Climate Algorithm Theoretical Basis Document
CCM3	Community Climate Model-3
CDR	Climate Data Record
EUMETSAT	European Organisation for the Exploitation of Meteorological Satellites
FOV	Field of View
MSU	Microwave Sounding Unit
NASA	National Aeronautics and Space Administration
NCDC	National Climatic Data Center
NCEP	National Center for Environmental Prediction
NOAA	National Oceanic and Atmospheric Administration
RSS	Remote Sensing Systems
TLS	Temperature Lower Stratosphere
TLT	Temperature Lower Troposphere
TMT	Temperature Middle Troposphere
TTS	Temperature Troposphere Stratosphere